Fabrication of nanodiamond reinforced aluminum composite coatings by flame spraying for marine applications

Yaoyao Fu[a,b], Xiuyong Chen[a,*], Botao Zhang[c], Yongfeng Gong[a], Haijun Zhang[a], Hua Li[a,*]

[a] Key Laboratory of Marine Materials and Related Technologies, Zhejiang Key Laboratory of Marine Materials and Protective Technologies, Ningbo Institute of Materials Technology and Engineering, Chinese Academy of Sciences, Ningbo 315201, China
[b] University of Chinese Academy of Sciences, Beijing 100049, China
[c] Cixi Institute of Biomedical Engineering, Ningbo Institute of Materials Technology and Engineering, Chinese Academy of Sciences, Ningbo 315201, China

ARTICLE INFO

ABSTRACT

Thermal sprayed aluminum (Al) coatings have been extensively utilized for marine anticorrosion applications. However, lack in mechanical strength of the coatings persists as a big concern for their long-term service in harsh marine environment. In this study, nanodiamond (ND) reinforced Al metal matrix composite coatings with enhanced mechanical properties were fabricated by flame spraying the mixture of micron-sized Al powder and ND suspension for the first time. Microstructural characterization and assessment of mechanical/corrosion properties of the Al-ND composite coatings were conducted. Results show that the coatings with perfectly retained ND exhibit reduced porosity and increased hardness, exhibiting remarkably enhanced anti-corrosion and anti-wear performances. The study presents a promising way to develop ND reinforced metal matrix composite coatings for potential marine applications.

1. Introduction

Surface engineering is one of the most effective methods to reduce corrosion damage of marine structures. Among numerous techniques, thermal sprayed Al coatings have been widely adopted in both laboratories and industries due to their excellent anti-corrosion property [1]. However, further enhancement of their wear resistance performances are still needed since marine corrosion always accompanies wear [2,3]. To produce Al coatings with outstanding mechanical properties, nanomaterials with superior physiochemical properties have been extensively used as reinforcement [4–7]. Searching for efficient methods to fabricate novel Al-based composite coatings with combined corrosion/wear resistance is one of the major goals of current research.

Due to its unique properties such as supreme hardness, high Young's modulus, low frictional coefficient and high surface energy [8,9], nanodiamond (ND) has been widely employed as reinforcement phase for different types of materials including metals [10], polymers [11] and ceramics [12]. Many attempts were made recently in constructing ND reinforced composite coatings by thermal spray approaches. ND composite coatings with nylon [13], copper [14,15], aluminum [16] have been fabricated by HVOF [13], plasma spray [17], or cold spray [10], etc. For the coating deposition, Al-ND composite powder could be firstly synthesized by means of high energy ball milling and the effect of milling time and ND content on the structure and properties of resulting MMC powders were systematically studied [16], and then dense Al-ND composite coating with higher hardness and elastic modulus than the starting Al-ND powder was developed by low pressure cold spray [10]. In addition, Al-Si-ND composite coatings were fabricated by plasma spraying [17]. The ND reinforced Al-Si coatings showed great potential as wear resistant coatings with lower coefficient of friction and higher microhardness. Although the mechanical performance of the as-sprayed coatings was significantly enhanced with ND reinforcement, additional steps such as synthesis of composite powder using mechanical alloying is necessary to obtain composite coatings via conventional thermal spray process. In addition, ND particles usually suffer oxidization and graphitizing during the high temperature deposition processing. As a relatively new coating fabrication method, suspension thermal spray utilizes the feedstock in the form of suspension which is particularly suitable for depositing nanoparticles [18–20]. Recently, we have proposed a plasma spray route using a feedstock mixing suspension and dry powder simultaneously for fabricating novel ND reinforced hydroxyapatite composite coatings [21], providing the possibilities of constructing nanosized particle reinforced metal matrix composite coatings.

In this study, we fabricated ND-reinforced Al coatings by a flame spraying route. Different from conventional solid or liquid/suspension

---

* Corresponding authors.
E-mail addresses: chenxiuyong@nimte.ac.cn (X. Chen), lihua@nimte.ac.cn (H. Li).
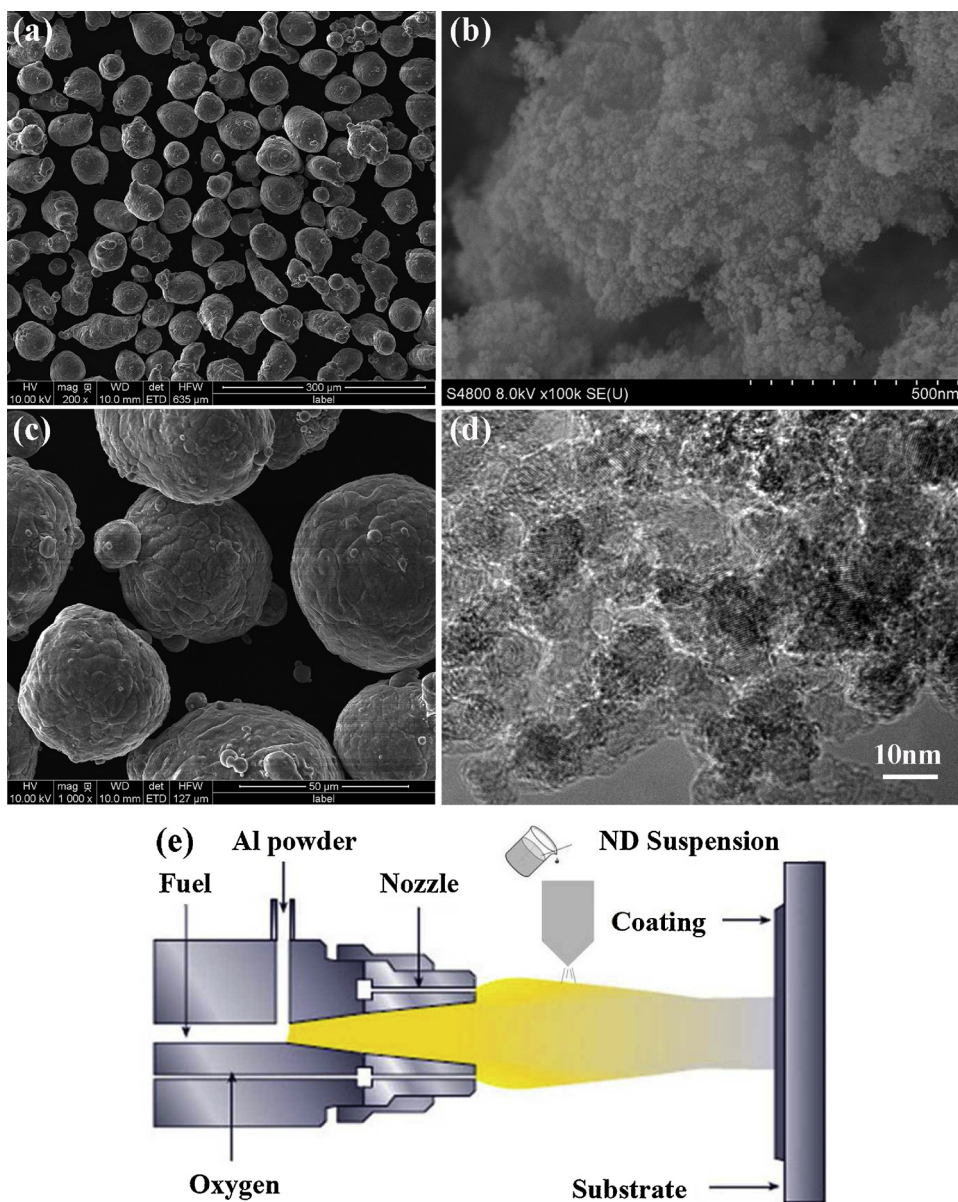
Fig. 1. SEM images of the starting Al (a) and the ND powder (b), (c) enlarged SEM view of the Al powder, (d) TEM image of the ND particles, and (e) schematic depiction of the flame spraying process.
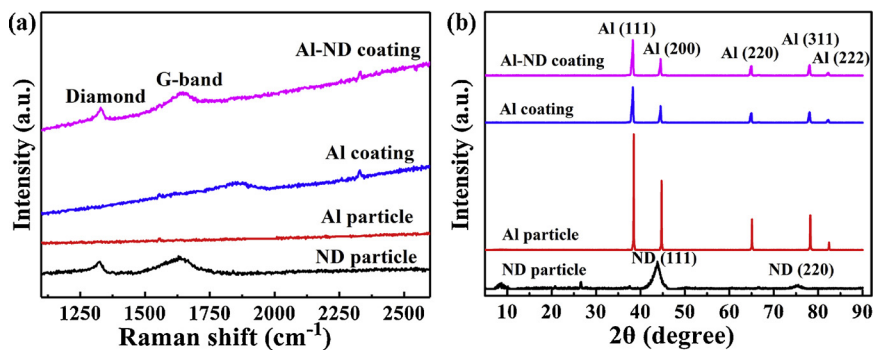

Fig. 2. Raman spectra (a) and XRD diffraction patterns (b) of the starting powder and the as-sprayed coatings.

flame spraying processes, Al powder and ND suspension were separately fed into the flame torch simultaneously. The effects of ND reinforcement on microstructure, mechanical and corrosion performances of the coatings were investigated.

2. Materials and methods

Micron-sized Al powder with particle size of 38–74 μm (Tianjiu Inc. Changsha, China) was used. The starting Al powder shows near
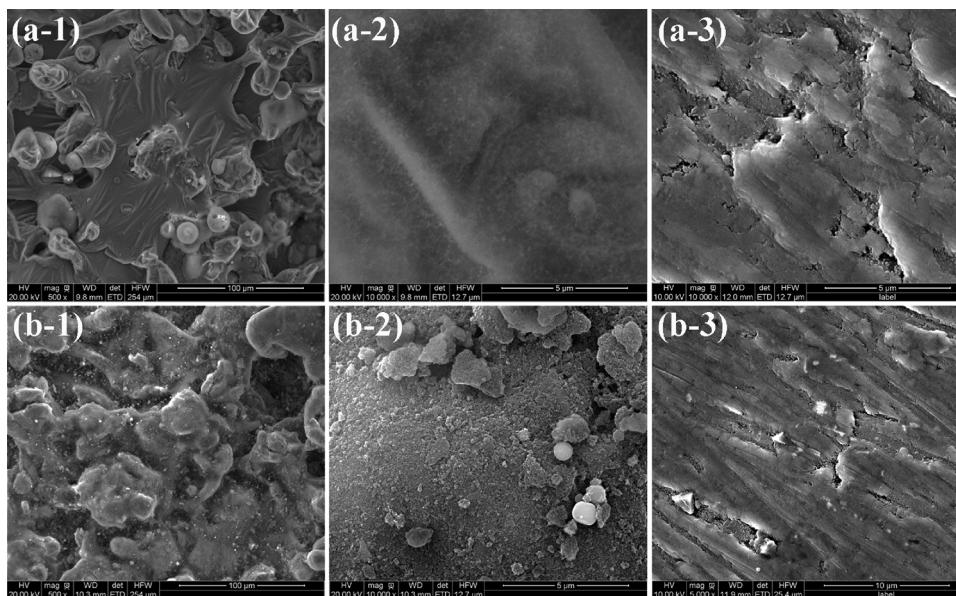
Fig. 3. SEM images of the Al coating (a) and the Al-ND composited coating (b) (-2 is enlarged view of selected area in -1, -3 is cross-sectional view of the coating).
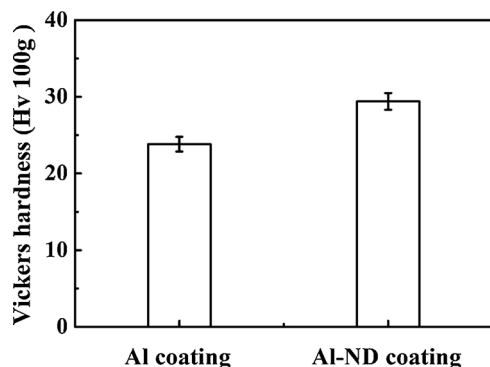

Fig. 4. Vickers hardness of the as-sprayed coatings.

spherical contour of the particles with an average diameter of ~50 μm (Fig. 1a and c), which has favorable fluidity for being fed into flame torch. ND particles with the size range of 5–10 nm were provided by Nafortis Inc. (Shanghai, China). Following sonochemical dispersion by bead assisted sonic disintegration in ice-bath, freeze drying and heat treatment at 450 °C for 2 h were carried out to obtain ultra-dispersed and ultra-pure ND particles [22]. Briefly, in the sonochemical dispersion process, 30～50 μm microsized diamond particles were added into nanodiamond suspension and stirred at high speed by a sonicator probe. Homogeneously dispersed nanodiamond suspension was obtained owing to the impact and shear force in the collision. Further heat

treatment was conducted to remove nondiamond carbon under ambient atmosphere in a tube furnace, which contained three steps: (i) gradual heating at 5 °C/min to 450 °C, (ii) isothermal oxidation for 2 h at 450 °C, and (iii) gradual cooling under ambient atmosphere. The purified ND particles were then dispersed in deionized water for coating deposition. Clear aggregation of ND particles was observed because of the high surface energy and the existence of oxygen-containing groups on the detonation ND surface (Fig. 1b and d) [8]. TEM image of ND particles show clear diamond crystal lattice (Fig. 1d), indicating that the particle is diamond. Fig. 1e shows the scheme of the flame spray deposition of the Al-ND coating on steel substrates. The specially designed feeding system was expected to maintain the intrinsic physicochemical property of ND in the composite coatings, and the addition of ND into Al coatings could enhance their mechanical properties for protecting marine structures.

In this study, ND reinforced Al coatings were deposited by flame spray (CDS 8000, Castolin, UK) on mild steel substrates (20 × 20 × 2.5 mm). Prior to the spraying, ultrasonic decontamination in acetone, air-drying and subsequently grit blasting was carried out for the substrates to remove the organics and oxidation on their surfaces. Acetylene and oxygen with the pressure and flow rate of 0.1 MPa and 0.3 MPa, 0.30 m^3/h and 0.25 m^3/h, respectively, were used for the spraying. Compressed air with a pressure of 0.4 MPa was used to atomize and accelerate the feedstock. Al powder feed rate was ~4.0 g/min with and the spray distance was set at 250 mm. To fabricate Al-ND composite coatings, ND suspension (0.25 wt.%) was injected into the flame torch by the atomizing nozzle with a flow rate of 66.67 ml/min.
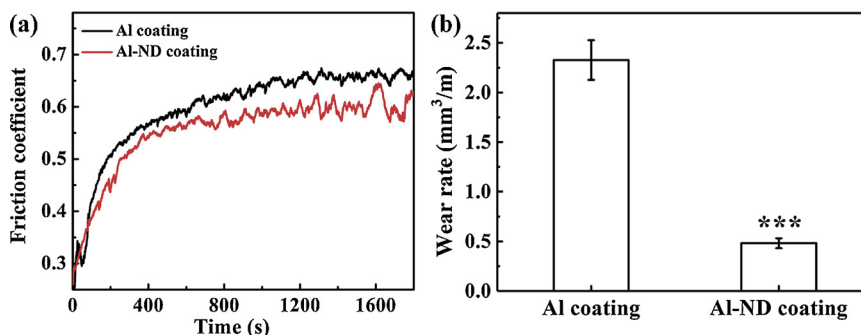

Fig. 5. Friction coefficients (a) and wear rates (b) of the coatings. Error bars represent means ± SD for n = 3, ***p < 0.001.
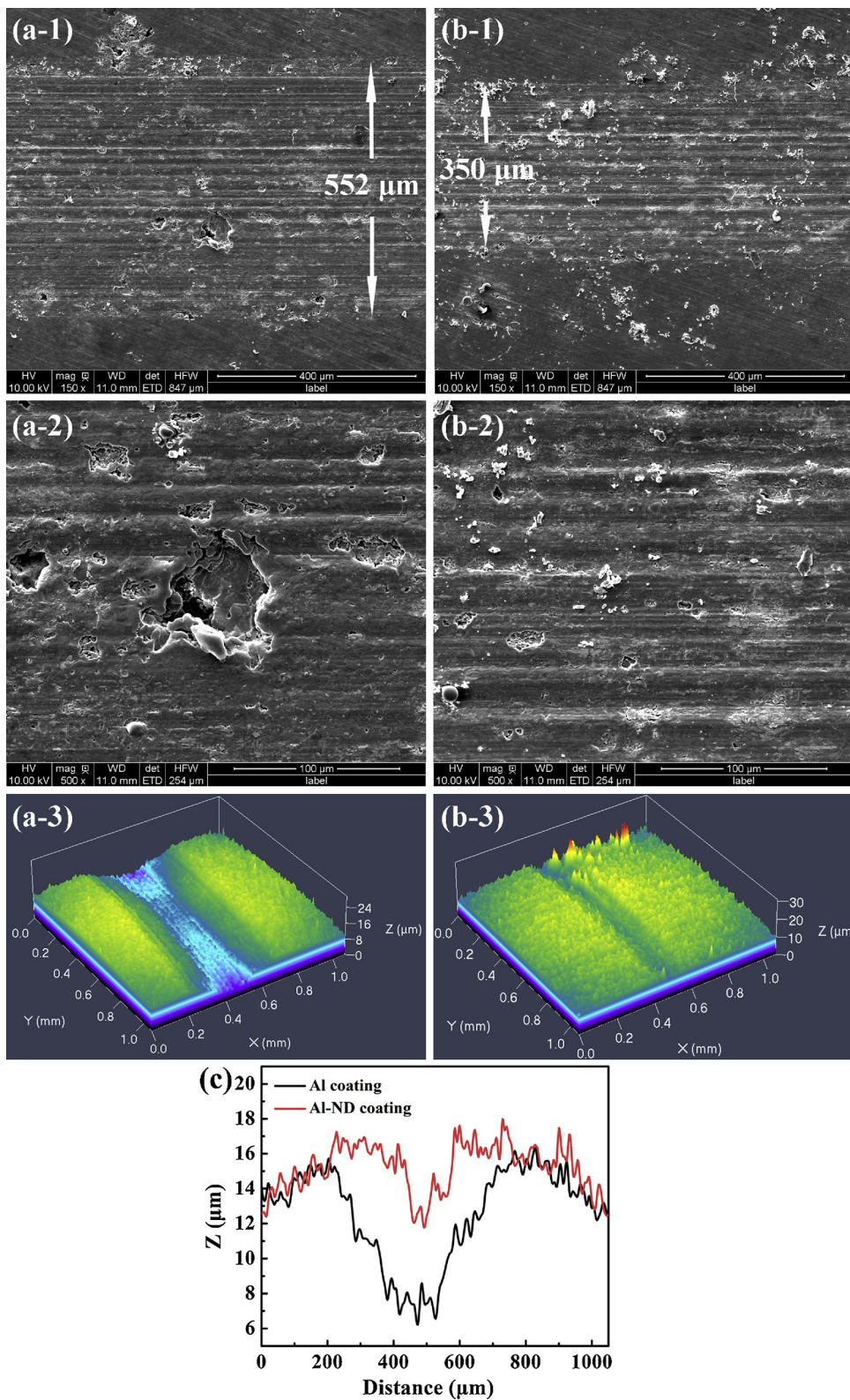
Fig. 6. SEM images of the wear track of the Al coating (a-1, a-2) and the Al-ND composited coating (b-1, b-2, -2 is the enlarged view of selected area in -1), 3D-morphlogy of the wear track of the Al coating (a-3) and the Al-ND composite coating (b-3), and (c) surface profile of the wear tracks of the coatings.

Field emission scanning electron microscopy (FE-SEM, Quanta FEG 250, USA) was used to observe the morphology of the starting powder and the as-sprayed coatings. High resolution transmission electron microscopy (HR-TEM, FEI Tecnai F20, USA) was employed to examine the crystal structure of ND particle. X-ray diffraction (XRD, Bruker D8 Advance Davinci, Germany) investigation of both the starting powder and the as-sprayed coatings was carried out using Cu Kα radiation ($\lambda = 1.54 \text{ Å}$) operated at 40 mA and 40 kV. Raman spectroscopy is a competitive method to analyze the structures of carbon nanomaterials [23]. In this study, we utilized Raman spectroscopy with a 325 nm
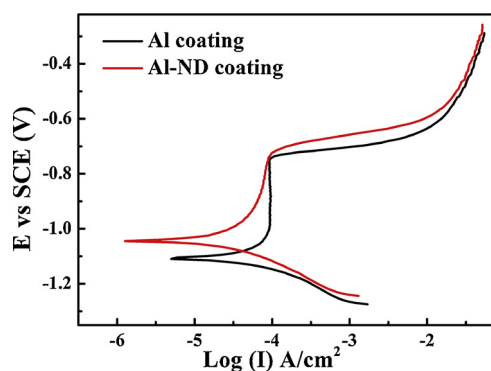
Fig. 7. Polarization curves of the as-sprayed coatings measured in 3.5 wt.% NaCl solution.

ultraviolet laser (Renishaw inVia-reflex, Britain) to determine the structural changes of ND during the coating deposition processing. Porosity of the coatings was measured by Brunauer, Emmett and Teller (BET, Micromeritics ASAP 2020 M, USA).

Hardness meter (HV-1000, China) with 100 g force was used to measure the Vickers microhardness of the coatings, and ten points for each sample were measured. Reciprocating type ball-on-disc tribometer (UMT-3, USA) was employed to evaluate the tribological properties of the coatings in room temperature 3.5 wt.% NaCl solution. The testing was conducted under 1.0 N load and a constant sliding velocity of 10 mm/s for 20 min. 316 L stainless steel balls (3 mm in diameter) acted as the counterpart, and a new ball was used for each time testing. During the friction testing, the friction coefficient and sliding time were recorded automatically. The testing for each sample was repeated three times for an average coefficient value. After the testing, three-dimensional surface profiler (Alpha-Step IQ, USA) was used to examine the wear rate according to the equation: $W = V/(F \times L)$, where W, V, F, L are the wear rate, wear volume, applied normal load and sliding distance, respectively. The average cross-sectional area of the wear track was estimated by integrating the wear track depth profiles using OriginPro (version 6.1), and the wear volume was calculated by multiplying the wear length and cross-sectional area of the wear track. For each calculation, five cross-sectional profiles were used to obtain an average value. Furthermore, FE-SEM was utilized to observe the topological morphological features of the wear tracks and confocal laser scanning microscopy (CLSM, Zeiss LSM 700, Germany) was used to depict the surface profiles of the wear tracks according to previous studies [24–26]. Corrosion resistance of the as-sprayed coatings was investigated by Tafel polarization testing in 3.5 wt.% NaCl solution using a commercial electrochemical workstation (Modulab, 2100 A, Britain). A traditional three-electrode cell was used. The as-sprayed coatings capsulated by resin with 1 cm^2 exposed area were working electrode, and saturated calomel electrode was used as the reference electrode and a 1 cm^2 platinum acted as the counter electrode. All the samples were immersed in NaCl solution for 1 h to reach the open circuit potential stabilization before electrochemical testing. The statistical analysis was performed with OriginPro (version 6.1) at confidence levels of 99.9%.

3. Results and discussion

Fig. 2a shows the Raman spectra of the starting powder and the as-sprayed coatings. ND particles display two characteristic Raman peaks at ~1328 cm^{-1} and 1500~1800 cm^{-1}. The peak at ~1328 cm^{-1} is assigned to diamond. The wide band of ND between 1500 and 1800 cm^{-1} normally refers to the G band [27,28], owning to the sp^2 carbon (~1590 cm^{-1}), O−H (~1640 cm^{-1}) and C=O (~1740 cm^{-1}) species [29]. It's worth noting that no D-band was observed in the Raman spectra, which might be due to the pre-treatment of the as-

received ND particles. Interestingly, the intensity of the Raman peaks of ND in the Al-ND composite coating did not significantly decrease than in ND particles, suggesting well retained ND structure in the composites. Sensitive response of ND to Raman signals and Raman inactive nature of Al are already well known. The well-retained structure of ND further suggests the feasibility of the coating fabrication approach for constructing ND-reinforced composites. XRD patterns of the starting powder and the as-sprayed coatings were also obtained (Fig. 2b). The peaks located at around 43° and 75° are attributed to the (111) and (200) crystal planes of diamond, and the feature of the broad peak indicates nanocrystalline characteristics of the ND particles [30]. It is noted that no XRD peak was detected for ND in the Al-ND coating, which is likely due to the relatively low content of ND in the coating. In addition, no alumina peaks were detected in the as-sprayed coatings, indicating negligible oxidation of Al during the deposition. The relatively high deposition rate of flame spraying and the evaporation of the solvent during the spraying predominately contribute to less heating of ND for retained diamond structure. The unique advantages of well control over the chemistry of the coatings are offered by the suspension thermal spraying [19–21].

To analyze the differences in microstructure between the Al and Al-ND coatings, their surface and cross-sectional morphologies were characterized by SEM (Fig. 3). The typical microstructure of the as-sprayed Al coating is shown in Fig. 3 a-1 and a-2. NDs are clearly seen in the Al-ND coating (Fig. 3b-1 vs -2). It was reported that the addition of ND led to a higher level of porosity in the high velocity oxy-fuel sprayed coatings but lower porosity in the air plasma sprayed coatings [31]. However, it should be noted that in this case, porosity of the coating can be significantly reduced by ND addition (Fig. 3a-3 vs b-3). Larger pores are present in the pure Al coating, while the Al-ND coating exhibits smaller pores as compared with the pure Al coating. Furthermore, porosity measurement by BET method showed the porosity of the Al coating and Al-ND composite coating of 3.31% and 1.35%, respectively. The reduced porosity would be due to the high specific surface area of ND nanoparticles, which would increase the specific contact area of the reinforcement and matrix, thus increasing healing of the pores at the reinforcement-matrix interface. This phenomenon can also be explained by possibly increased filling of spaces between bigger unmelted or semimelted Al particles by ND particles [32]. These results suggest that the suspension flame spray is suitable for making ND-reinforced metal matrix composites.

To meet the demand for protection from wear-associated corrosion in the environments like splash zone [33], sufficient hardness is also needed for thermal sprayed marine coatings to accomplish long-term functional services. Vickers hardness measurement was made in this study (Fig. 4), which is a widely used technique for hardness measurement [34]. The Al coatings alone displayed relatively low hardness with an average HV value of ~24. The hardness of the Al-ND coatings is much higher value than that of the Al coatings. This could be explained by the markedly reduced porosity of the coatings by the addition of ND. Moreover, the existence of high ND content diffusing between Al particles would further enhance the hardness of the Al coatings. This result is consistent with the data reported previously [10,16].

Furthermore, the influence of ND addition on the friction coefficient of the coatings was investigated (Fig. 5a). Regardless of the reduced porosities and the enhanced hardness of the Al-ND coatings, no statistically significant differences in friction coefficient were observed between the ND-free and the ND-incorporated coatings. However, significantly reduced wear rate was observed for the ND-reinforced coatings (Fig. 5b). Average wear rate of the Al-ND coatings is ~17.5% of that of the pure Al coatings. To further confirm the enhancement of the mechanical properties of the coatings by the addition of ND, morphology of the wear tracks were characterized using SEM and CLSM, respectively (Fig. 6). It is observed that morphology of the Al coating after abrasion is clearly different from that of the Al-ND coatings

(Fig. 6a vs b). Microcrack grooves and micro-ploughing are recognized on the worn surface of both the Al coating and the Al-ND coating, suggesting an abrasive wear-dominated regime [35]. However, there are a small amount of sticking points on the worn surface of the Al coating, and some areas are broken down and removed from the wear track (Fig. 6a-2), which suggests adhesive wear. In this case, only abrasive wear plays a role in regulating the wear of the Al-ND coating, but a combination of abrasive wear and adhesive wear decides the wear behaviors of the Al coating. Thus, the Al coating would be more severely abraded than the Al-ND coating. Furthermore, the CLSM images show that the wear track on the pure Al coating displays relatively wider and much deeper groove than those of the Al-ND coating (Fig. 6a-3 vs b-3), presumably owning to the lower hardness and higher wear rate of the coating. This is consistent with the wear rate result (Fig. 5b) and a previous study [36]. Further surface profile of the wear track of the as-sprayed coatings (Fig. 6c) evidenced the worn morphologies observed above, the width ($\sim 552\,\mu m$) and depth ($\sim 9\,\mu m$) of the wear tracks of the Al coating are much wider and deeper than those of the Al-ND coating ($\sim 350\,\mu m$ in width and $4\,\mu m$ in depth). The enhanced hardness of the coating would resist the abrasive medium penetrating into the coating matrix, and as a result, the amount of material on the coating surface removed by the friction counterpart could be decreased. Apart from the coating hardness, the polishing and rolling effect of ND particles has been clarified in a previous study [37]. The polishing effect could decrease the shear stress on the surface and the rolling effect could smooth the sliding wear property [38].

Lower porosity usually results in better corrosion resistant performance, leading to long-term protection for marine structures. The anti-corrosion properties of the Al-ND composite coatings were assessed by potentiodynamic polarization testing performed in 3.5 wt.% NaCl solution. As shown in Fig. 7, the corrosion potentials of the Al coating and the Al-ND coating are -1.116 V and -1.056 V, respectively. In addition, the corrosion current density of the Al coating, $3.97 \times 10^{-5}\,A/cm^2$, is much higher than that of the Al-ND coatings, $2.128 \times 10\text{-}5\,A/cm^2$. In general, a lower corrosion current density suggests a lower corrosion dynamic rate, and a higher corrosion potential implies less likeliness that the coating tends to be corroded [39,40]. Thus, the novel ND reinforced Al coatings with favorable anti-corrosion and enhanced mechanical properties have great potential for protecting marine structures.

4. Conclusions

In summary, we fabricated Al-ND composite coatings by flame spraying using a novel mixed feedstock of both suspension and dry powder. The structure of the ND particles was well retained in the Al-ND composite coatings. The addition of ND resulted in much lower porosity, in turn significantly enhanced mechanical properties of the Al coatings. More importantly, the corrosion resistance of the ND-reinforced composite coatings was markedly improved in comparison to the pure Al coatings. The present study provides a promising method for fabrication of nanomaterials reinforced metal matrix composite coatings against both corrosion and wear for potential marine applications.

Acknowledgments

References

[1] F.S.D. Silva, J. Bedoya, S. Dosta, N. Cinca, I.G. Cano, J.M. Guilemany, A.V. Benedetti, Corrosion characteristics of cold gas spray coatings of reinforced aluminum deposited onto carbon steel, Corros. Sci. 114 (2017) 57–71.

[2] J. Cheng, F. Li, S. Zhu, Y. Yu, Z. Qiao, J. Yang, Electrochemical corrosion and tribological evaluation of TiAl alloy for marine application, Tribol. Int. 115 (2017) 483–492.

[3] R.J.K. Wood, Marine wear and tribocorrosion, Wear 376 (2017) 893–910.

[4] S.R. Bakshi, A. Agarwal, An analysis of the factors affecting strengthening in carbon nanotube reinforced aluminum composites, Carbon 49 (2011) 533–544.

[5] R. Casati, M. Vedani, Metal matrix composites reinforced by nano-particles-a review, Metals 4 (2014) 65–83.

[6] C. He, N. Zhao, C. Shi, X. Du, J. Li, H. Li, Q. Cui, An approach to obtaining homogeneously dispersed carbon nanotubes in Al powders for preparing reinforced Al-matrix composites, Adv. Mater. 19 (2007) 1128–1132.

[7] H. Kwon, M. Estili, K. Takagi, T. Miyazaki, A. Kawasaki, Combination of hot extrusion and spark plasma sintering for producing carbon nanotube reinforced aluminum matrix composites, Carbon 47 (2009) 570–577.

[8] A. Kruger, F. Kataoka, M. Ozawa, T. Fujino, Y. Suzuki, A.E. Aleksenskii, A.Y. Vul, E. Osawa, Unusually tight aggregation in detonation nanodiamond: identification and disintegration, Carbon 43 (2005) 1722–1730.

[9] I. Neitzel, V. Mochalin, J.A. Bares, R.W. Carpick, A. Erdemir, Y. Gogotsi, Tribological properties of nanodiamond-epoxy composites, Tribol. Lett. 47 (2012) 195–202.

[10] D.J. Woo, F.C. Heer, L.N. Brewer, J.P. Hooper, S. Osswald, Synthesis of nanodiamond-reinforced aluminum metal matrix composites using cold-spray deposition, Carbon 86 (2015) 15–25.

[11] V.N. Mochalin, I. Neitzel, B.J.M. Etzold, A. Peterson, G. Palmese, Y. Gogotsi, Covalent incorporation of aminated nanodiamond into an epoxy polymer network, ACS Nano 5 (2011) 7494–7502.

[12] A. Nieto, L. Jiang, J. Kim, D.E. Kim, J.M. Schoenung, Synthesis and multi scale tribological behavior of WC-Co/nanodiamond nanocomposites, Sci. Rep. UK 7 (2017) 7060.

[13] A. Stravato, R. Knight, V. Mochalin, S.C. Picardi, HVOF-sprayed nylon-11 + nanodiamond composite coatings: production & characterization, J. Therm. Spray Technol. 17 (2008) 812–817.

[14] V.A. Popov, L.S. Belevsky, E.L. Belevskaya, I.M. Gordon, S.A. Tulupov, A new method for production of a copper coating reinforced with nano-diamonds, J. Alloys 434-435 (2007) 689–692.

[15] V. Livramento, J.B. Correia, N. Shohoji, E. Osawa, Nanodiamond as an effective reinforcing component for nano-copper, Diamond Relat. Mater. 16 (2007) 202–204.

[16] D.J. Woo, B. Sneed, F. Peerally, F.C. Heer, L.N. Brewer, J.P. Hooper, S. Osswald, Synthesis of nanodiamond-reinforced aluminum metal composite powders and coatings using high-energy ball milling and cold spray, Carbon 63 (2013) 404–415.

[17] M. Bao, C. Zhang, D. Lahiri, A. Agarwal, The tribological behavior of plasma-sprayed Al-Si composite coatings reinforced with nanodiamond, JOM 64 (2012) 702–708.

[18] X. Chen, Y. Gong, D. Li, H. Li, Robust and easy-repairable superhydrophobic surfaces with multiple length-scale topography constructed by thermal spray route, Colloids Surf. A: Physicochem. Eng. Asp. 492 (2016) 19–25.

[19] X. Chen, J. Yuan, J. Huang, K. Ren, Y. Liu, S. Lu, H. Li, Large-scale fabrication of superhydrophobic polyurethane/nano-Al₂O₃ coatings by suspension flame spraying for anti-corrosion applications, Appl. Surf. Sci. 311 (2014) 864–869.

[20] M. Zhai, Y. Gong, X. Chen, T. Xiao, G. Zhang, L. Xu, H. Li, Mass-producible hydrophobic perfluoroalkoxy/nano-silver coatings by suspension flame spraying for antifouling and drag reduction applications, Surf. Coat. Technol. 328 (2017) 115–120.

[21] X. Chen, B. Zhang, Y. Gong, P. Zhou, H. Li, Mechanical properties of nanodiamond-reinforced hydroxyapatite composite coatings deposited by suspension plasma spraying, Appl. Surf. Sci. 439 (2018) 60–65.

[22] S. Osswald, G. Yushin, V. Mochalin, S.O. Kucheyev, Y. Gogotsi, Control of sp²/sp³ carbon ratio and surface chemistry of nanodiamond powders by selective oxidation in air, J. Am. Chem. Soc. 128 (2006) 11635–11642.

[23] M.L. Gupta, S.A. Sydlik, J.M. Schnorr, D.J. Woo, S. Osswald, T.M. Swager, D. Raghavan, The effect of mixing methods on the dispersion of carbon nanotubes during the solvent-free processing of multiwalled carbon nanotube/epoxy composites, J. Polym. Sci. Polym. Phys. Ed. 51 (2013) 410–420.

[24] H. Kumar, V. Ramakrishnan, S.K. Albert, A.K. Bhaduri, K.K. Ray, Friction and wear behaviour of Ni-Cr-B hardface coating on 316LN stainless steel in liquid sodium at elevated temperature, J. Nucl. Phys. Mater. Sci. Radiat. Appl. 495 (2017) 431–437.

[25] Z. Li, X. Guan, Y. Wang, J. Li, X. Cheng, X. Lu, L. Wang, Q. Xue, Comparative study on the load carrying capacities of DLC, GLC and CrN coatings under sliding-friction condition in different environments, Surf. Coat. Technol. 321 (2017) 350–357.

[26] Z. Wang, J. Ni, D. Gao, Combined effect of the use of carbon fiber and seawater and the molecular structure on the tribological behavior of polymer materials, Friction 6 (2018) 183–194.

[27] A.C. Ferrari, J. Robertson, Raman spectroscopy of amorphous, nanostructured, diamond-like carbon, and nanodiamond, Philos. Trans. Math. Phys. Eng. Sci. 362 (2004) 2477–2512.

[28] S. Osswald, V.N. Mochalin, M. Havel, G. Yushin, Y. Gogotsi, Phonon confinement effects in the raman spectrum of nanodiamond, Phys. Rev. B 80 (2009) 075419.

[29] V. Mochalin, S. Osswald, Y. Gogotsi, Contribution of functional groups to the raman spectrum of nanodiamond powders, Chem. Mater. 21 (2009) 273–279.

[30] V.Y. Shevchenko, A.E. Madison, G.S. Yur'ev, Structure of nanodiamonds, Glass Phys. Chem. 32 (2006) 261–266.

[31] P. Fauchais, A. Vardelle, B. Dussoubs, Quo vadis thermal spraying? J. Therm. Spray Technol. 10 (2001) 44–66.

[32] S. Mahato, S.K. Pratihar, S.K. Behera, Fabrication and properties of MgO–C

refractories improved with expanded graphite, Ceram. Int. 40 (2014) 16535–16542.

[33] S. Kuroda, J. Kawakita, M. Takemoto, An 18-year exposure test of thermal-sprayed Zn, Al, and Zn-Al coatings in marine environment, Corrosion 62 (2006) 635–647.

[34] M.R. Ayatollahi, E. Alishahi, S. Doagou R, S. Shadlou, Tribological and mechanical properties of low content nanodiamond/epoxy nanocomposites, Compos. Part B: Eng. 43 (2012) 3425–3430.

[35] J. Park, S.H. You, D.W. Shin, A. Ozturk, Tribological behavior of alumina-added apatite-wollastonite glass-ceramics in simulated body fluid, Mater. Chem. Phys. 124 (2010) 113–119.

[36] A.R. Molla, B.V.M. Kumar, B. Basu, Friction and wear mechanisms of K_2O-B_2O_3-Al_2O_3-SiO_2-MgO-F glass-ceramics, J. Eur. Ceram. Soc. 29 (2009) 2481–2489.

[37] Y. Zhu, Z. Feng, B. Wang, X. Xu, Dispersion of nanodiamond and ultra-fine polishing of quartz wafer, China Particuol. 2 (2004) 153–156.

[38] R.S. Dwyerjoyce, R.S. Sayles, E. Ioannides, An investigation into the mechanisms of closed three-body abrasive wear, Wear 175 (1994) 133–142.

[39] H.M. Ezuber, A. Elhoud, F. Elshawesh, A study on the corrosion behavior of aluminum alloys in seawater, Mater. Des. 29 (2008) 801–805.

[40] G. Song, M. Liu, Corrosion and electrochemical evaluation of an Al-Si-Cu aluminum alloy in ethanol solutions, Corros. Sci. 72 (2013) 73–81.